Transport and Communications Science Journal

PHASE-FIELD BASED FREE VIBRATION ANALYSIS OF CRACKED POROUS COMPOSITE PLATES WITH PARABOLICALLY VARYING THICKNESS ON ELASTIC FOUNDATIONS

Pham Minh Phuc

University of Transport and Communications, No 3 Cau Giay Street, Hanoi, Vietnam

ARTICLE INFO

TYPE: Research Article
Received: 22/12/2025
Revised: 17/04/2026
Accepted: 10/05/2026
Published online: 15/05/2026
https://doi.org/10.47869/tcsj.77.4.1
* *Corresponding author*
Email: phamminhphuc@utc.edu.vn

Abstract. Composite plates with cracks, variable thickness, and porous structures are increasingly used in modern engineering applications due to their superior performance under complex operating conditions. However, the combined effects of porosity, variable thickness, cracks, and elastic foundation on the free vibration behavior of such plates are still not fully understood. This study investigates the free vibration characteristics of a porous functionally graded plate with parabolically varying thickness along the x-axis. A crack is assumed to be located either at the center or at the edge of the plate. The material porosity is considered to be uniformly distributed through the plate thickness. The governing equations are established based on the first-order shear deformation theory in combination with the phase-field approach to simulate the crack behavior. The finite element method is employed to solve the resulting eigenvalue problem and obtain the natural frequencies of the plate. Parametric studies are carried out to examine the influences of crack length, crack position, porosity coefficient, thickness variation, and elastic foundation stiffness on the vibration response. The numerical results demonstrate that the crack length and crack location have a significant effect on the natural frequencies, while the presence of a stiff elastic foundation remarkably reduces the sensitivity of the vibration characteristics to cracking effects.

Keywords: Porous material, functionally graded plate, variable thickness, crack, Phase-field, elastic foundation.

1. INTRODUCTION

Composite plates composed of ceramic and metal constituents, known as functionally graded (FG) materials, have been widely used in modern engineering due to their smooth variation of material properties and their ability to overcome delamination problems commonly observed in layered composites. The gradual change in stiffness, density, and thermal properties enhances structural performance under severe thermal and mechanical environments, making FG plates suitable for aerospace, mechanical, and civil engineering applications. Since many of these components operate under dynamic loads, the vibration behaviour of FG plates has received significant attention, and numerous studies have analysed their free vibration responses using various refined plate theories and numerical techniques [1-5].

In practical engineering, however, plates often exhibit non-uniform thickness rather than a constant one. Thickness variation may arise from design requirements or manufacturing constraints and leads to spatially varying stiffness and mass distributions, thereby significantly influencing dynamic characteristics. Early investigations employed classical and shear deformation theories to analyse the vibration behaviour of variable-thickness plates [6]. Later, more advanced techniques, including the Rayleigh–Ritz method, extended Kantorovich method, and differential transformation method, were developed to enhance accuracy for plates with complex thickness variations [7-9]. With the advancement of computational methods, isogeometric analysis, meshless schemes, and finite element formulations have been used to study FG plates with variable thickness, demonstrating strong coupling between geometric non-uniformity and material gradation [8-10]. These studies collectively confirm that even small thickness variations can cause noticeable changes in natural frequencies.

Along with geometric variation, structural defects such as cracks are unavoidable due to fatigue, impact, or harsh working conditions. Cracks reduce stiffness and may significantly alter vibration behaviour. For FG plates, crack effects interact with material gradation, making the problem more complex. Numerical approaches such as the finite element method, extended finite element method, and Ritz solutions have been widely employed to investigate cracked plates [10-14]. In recent years, the phase-field method has emerged as a robust approach for modelling crack initiation and growth without explicitly tracking crack surfaces. Studies coupling the phase-field model with shear deformation theories have shown that crack length and location have substantial effects on natural frequencies, particularly when cracks are near the plate center or boundaries [10-13].

Besides cracks and thickness variation, material porosity is another important factor influencing the mechanical performance of FGs. Porous FGs offer advantages such as reduced weight and enhanced thermal insulation but suffer from stiffness reduction that affects dynamic responses. Numerous studies have examined the vibration behaviour of porous FG plates with different porosity distributions using refined plate theories and numerical methods [15-18]. These studies show that increasing porosity typically decreases natural frequencies, while elastic foundations may partially compensate this effect. Porous plates have also been analysed under various geometrical configurations and environmental conditions, highlighting their engineering relevance.

Elastic foundations, commonly represented by Winkler or Pasternak models, play an essential role in supporting composite plate structures in many engineering applications. Previous studies have shown that the presence of elastic foundations increases system

stiffness and raises natural frequencies [12-18]. When porosity, cracks, and thickness variation coexist in composite plates, the dynamic behaviour becomes highly complex due to competing stiffness-reducing and stiffness-enhancing mechanisms. However, most available studies consider these effects separately rather than simultaneously.

A review of existing literature shows that although extensive work has been carried out on variable-thickness plates [6-10], cracked plates [10-14], and porous FG plates [15-18], comprehensive studies combining variable thickness, cracks, porosity, and elastic foundation effects remain scarce. In particular, no existing work has simultaneously investigated composite plates with parabolically varying thickness, uniformly distributed porosity, and centrally or edge-located cracks resting on elastic foundations. Moreover, the combined use of first-order shear deformation theory, the phase-field method for crack modelling, and finite element analysis for such complex composite plates has not been fully explored. This gap provides the primary motivation for the present study.

2. GOVERNING EQUATIONS

In this study, the FG plate possesses a thickness that varies only along the x-direction, as shown in Figure 1. The material gradation is defined so that the bottom surface is fully metallic, while the top surface is entirely ceramic. The variation of material properties through the thickness is governed by a power-law distribution expressed as follows:

$$V_m = 1 - V_c \; ; \quad V_c = \left(\frac{z}{h(x)} + \frac{1}{2} \right)^k \; ; \text{ with } k \geq 0 \tag{1}$$

The Young's moduli of the ceramic and metal constituents are denoted by E_c and E_m. The thickness varies as $h(x)$, while the material gradation is governed by the volume fraction index k, and e is the porosity coefficient of the plate material. The effective modulus $E(z)$ and Poisson's ratio $\upsilon(z)$ follow the power-law distribution:

$$\begin{Bmatrix} E(z) \\ \upsilon(z) \\ \rho(z) \end{Bmatrix} = \begin{Bmatrix} E_m \\ \upsilon_m \\ \rho_m \end{Bmatrix} + \left(\frac{z}{h(x)} + \frac{1}{2} \right)^k \begin{Bmatrix} E_c - E_m \\ \upsilon_c - \upsilon_m \\ \rho_c - \rho_m \end{Bmatrix} - \frac{e}{2} \begin{Bmatrix} E_c + E_m \\ \upsilon_c + \upsilon_m \\ \rho_c + \rho_m \end{Bmatrix} \tag{2}$$

The finite element formulation adopted here is based on FSDT and uses a kinematic model extracted from 3D elasticity rather than assumed displacement fields. Thus, the displacement (V_x, V_y, V_z) at any point (x, y, z) is described by five independent variables:

$$\begin{aligned} V_x(x,y,z,t) &= u_0(x,y,t) + z\theta_x(x,y,t) \\ V_y(x,y,z,t) &= v_0(x,y,t) + z\theta_y(x,y,t) \\ V_z(x,y,z,t) &= w_0(x,y,t) \end{aligned} \tag{3}$$

where, mid-surface displacements are denoted u_0, v_0, w_0, while θ_x and θ_y represent rotations about the y- and x-axes.

The discretization employs triangular elements with three nodes per element. Each node is assigned five structural degrees of freedom together with the phase-field variable s. The corresponding field variables are interpolated using finite element shape functions as shown below:

$$u_0 = \sum_{i=1}^{m} N_i u_{0i};\ v_0 = \sum_{i=1}^{m} N_i v_{0i};\ \theta_x = \sum_{i=1}^{m} N_i \theta_{xi};\ \theta_y = \sum_{i=1}^{m} N_i \theta_{yi} \tag{4}$$

where m = 3 indicates the number of element nodes, while N_i and N_i^s is denote the shape functions associated with the displacement variables and the phase-field variable.

The strain field of the plate is expressed as follows:

$$\begin{Bmatrix} \boldsymbol{\varepsilon} \\ \boldsymbol{\gamma} \end{Bmatrix} = \begin{Bmatrix} \boldsymbol{\varepsilon}_p \\ \mathbf{0} \end{Bmatrix} + \begin{Bmatrix} z\boldsymbol{\varepsilon}_b \\ \boldsymbol{\gamma}_s \end{Bmatrix} \tag{5}$$

where

$$\boldsymbol{\varepsilon}_p = \begin{Bmatrix} \dfrac{\partial u_0}{\partial x} \\ \dfrac{\partial v_0}{\partial y} \\ \dfrac{\partial v_0}{\partial x} + \dfrac{\partial u_0}{\partial y} \end{Bmatrix} = \boldsymbol{B}_0 \boldsymbol{d}_e;\quad \boldsymbol{\varepsilon}_b = \begin{Bmatrix} \dfrac{\partial \theta_x}{\partial x} \\ \dfrac{\partial \theta_y}{\partial y} \\ \dfrac{\partial \theta_y}{\partial x} + \dfrac{\partial \theta_x}{\partial y} \end{Bmatrix} = \boldsymbol{B}_1 \boldsymbol{d}_e;\quad \boldsymbol{\gamma}_s = \begin{Bmatrix} \dfrac{\partial \mathrm{w}_0}{\partial x} + \theta_x \\ \dfrac{\partial \mathrm{w}_0}{\partial y} + \theta_y \end{Bmatrix} = \boldsymbol{B}_s \boldsymbol{d}_e \tag{6}$$

with

$$\boldsymbol{B}_0 = \sum_{i=1}^{m} \begin{bmatrix} \dfrac{\partial N_i}{\partial x} & 0 & 0 & 0 & 0 \\ 0 & \dfrac{\partial N_i}{\partial y} & 0 & 0 & 0 \\ \dfrac{\partial N_i}{\partial y} & \dfrac{\partial N_i}{\partial x} & 0 & 0 & 0 \end{bmatrix};\qquad \boldsymbol{B}_1 = \sum_{i=1}^{m} \begin{bmatrix} 0 & 0 & 0 & \dfrac{\partial N_i}{\partial x} & 0 \\ 0 & 0 & 0 & 0 & \dfrac{\partial N_i}{\partial y} \\ 0 & 0 & 0 & \dfrac{\partial N_i}{\partial y} & \dfrac{\partial N_i}{\partial x} \end{bmatrix} \tag{7}$$

$$\boldsymbol{B}_s = \sum_{i=1}^{m} \begin{bmatrix} 0 & 0 & \dfrac{\partial N_i}{\partial x} & 1 & 0 \\ 0 & 0 & \dfrac{\partial N_i}{\partial y} & 0 & 1 \end{bmatrix} \quad \text{and} \quad \boldsymbol{d}_e = \left\{ u_0, v_0, w_0, \theta_x, \theta_y \right\}^T$$

The constitutive stress–strain relations are given by:

$$\begin{Bmatrix} \sigma \\ \tau \end{Bmatrix} = \begin{bmatrix} \boldsymbol{D}_m & 0 \\ 0 & \boldsymbol{D}_s \end{bmatrix} \begin{Bmatrix} \boldsymbol{\varepsilon} \\ \boldsymbol{\gamma} \end{Bmatrix} \tag{8}$$

The strain energy of the plate is written as:

$$U(\boldsymbol{d}) = \frac{1}{2} \int_{\Omega} s^2 \left\{ \boldsymbol{\varepsilon}_p^T \mathbf{A} \boldsymbol{\varepsilon}_p + \boldsymbol{\varepsilon}_p^T \mathbf{B} \boldsymbol{\varepsilon}_b + \boldsymbol{\varepsilon}_b^T \mathbf{B} \boldsymbol{\varepsilon}_p + \boldsymbol{\varepsilon}_b^T \mathbf{D}_b \boldsymbol{\varepsilon}_b + \boldsymbol{\gamma}_s^T \mathbf{D}_s \boldsymbol{\gamma}_s \right\} d\Omega \tag{9}$$

where

$$\boldsymbol{D}_m = \frac{E(z)}{1-\upsilon^2} \begin{bmatrix} 1 & \upsilon & 0 \\ \upsilon & 1 & 0 \\ 0 & 0 & \dfrac{1}{2}(1-\upsilon) \end{bmatrix};\qquad \boldsymbol{D}_s = \frac{5E(z)h}{12(1+\upsilon)} \begin{bmatrix} 1 & 0 \\ 0 & 1 \end{bmatrix} \tag{10}$$

$$\text{and} \quad (\boldsymbol{A},\boldsymbol{B},\boldsymbol{D}_b)=\int_{-h/2}^{h/2}(1,z,z^2)\boldsymbol{D}_m dz\,; \qquad \boldsymbol{d}=\sum \boldsymbol{d}_e \tag{11}$$

In the phase-field formulation for fracture, material degradation is represented through a scalar variable *s* that varies continuously between 0 and 1. A value close to 1 corresponds to undamaged material, whereas values approaching 0 indicate complete loss of load-carrying capacity. Intermediate values describe regions where the mechanical response is progressively weakened as damage develops. Under this description, a crack is no longer introduced as a geometric discontinuity; instead, it emerges as a narrow band in which the variable *s* transitions smoothly from intact to fully damaged states.

This continuous representation eliminates the need to explicitly trace crack surfaces, allowing derivatives and integrals to be computed over the entire domain without special treatment of discontinuities. Consequently, the initiation and evolution of micro-damage can be modeled in a natural manner within the same variational framework. In the present study, the phase-field variable is incorporated into the strain-energy density of the plate, reducing the elastic stiffness in regions where damage is present, as reflected in Eqs. (12)-(14). Through this mechanism, the formulation captures the gradual reduction in material stiffness that accompanies crack propagation.

Strain energy in the presence of a crack [10]:

$$\begin{aligned} U(\boldsymbol{d},s) &= \left\{ \begin{array}{l} \frac{1}{2}\int_\Omega s^2 \left\{ \boldsymbol{\varepsilon}_p^T \mathbf{A} \boldsymbol{\varepsilon}_p + \boldsymbol{\varepsilon}_p^T \mathbf{B} \boldsymbol{\varepsilon}_b + \boldsymbol{\varepsilon}_b^T \mathbf{B} \boldsymbol{\varepsilon}_p + \boldsymbol{\varepsilon}_b^T \mathbf{D} \boldsymbol{\varepsilon}_b + \boldsymbol{\gamma}_s^T \mathbf{D}_s \boldsymbol{\gamma}_s \right\} d\Omega + \\ + \int_\Omega G_C h \left[\frac{(1-s)^2}{4\ell_c} + \ell_c \left| \nabla s \right|^2 \right] d\Omega \end{array} \right\} \\ &= \left\{ \int_\Omega s^2 \varphi(\boldsymbol{d})\, d\Omega + \int_\Omega G_C h \left[\frac{(1-s)^2}{4\ell_c} + \ell_c \left| \nabla s \right|^2 \right] d\Omega \right\} \end{aligned} \tag{12}$$

Here, G_c is the Griffith critical energy release rate, and ℓ_c is a length-scale constant defining the width of the damage zone.

Expression for the plate's kinetic energy:

$$T(\boldsymbol{d},s)=\frac{1}{2}\int_V s^2 \rho(z)\left(\dot{V}_x^2+\dot{V}_y^2+\dot{V}_z^2\right)dV \tag{13}$$

For the Pasternak elastic foundation case, the foundation-induced strain energy takes the form:

$$U_{elas}(\boldsymbol{d},s)=\frac{1}{2}\int_\Omega s^2 \left\{ k_w w_0^2 + k_s \left[\left(\frac{\partial w_0}{\partial x} \right)^2 + \left(\frac{\partial w_0}{\partial y} \right)^2 \right] \right\} d\Omega \tag{14}$$

Here, k_w specifies the Winkler vertical stiffness, while k_s indicates the Pasternak shear stiffness.

Based on the derived expressions, the Lagrangian for the FG plate is expressed as:

$$\begin{aligned} L_a(\boldsymbol{d},s) &= T(\boldsymbol{d},s) - \left[U_t(\boldsymbol{d},s) + U_{elas}(\boldsymbol{d},s)\right] \\ &= \left\{ \int_{\boldsymbol{\Omega}} s^2\, \boldsymbol{\Phi}(\boldsymbol{d})\, d\boldsymbol{\Omega} - \int_{\boldsymbol{\Omega}} G_C h \left[\frac{(1-s)^2}{4\ell_c} + \ell_c \left|\nabla s\right|^2 \right] d\boldsymbol{\Omega} \right\} \end{aligned} \tag{15}$$

The first-order variation of $L(\boldsymbol{d},s)$ with respect to $\boldsymbol{d}$ and s is given by:

$$\begin{cases} \delta L_a(\boldsymbol{d},s,\delta\boldsymbol{d}) = \left(\sum \mathbf{K}^e + \boldsymbol{\omega}^2 \sum \boldsymbol{M}^e\right)\boldsymbol{d} = 0 & (16) \\ \delta L_a(\boldsymbol{d},s,\delta s) = \int_{\boldsymbol{\Omega}} 2s\,\Phi(\boldsymbol{d})\,\delta s\, d\boldsymbol{\Omega} - \int_{\boldsymbol{\Omega}} 2G_C h \left[\frac{(s-1)\delta s}{4\ell_c} + \ell_c \nabla s \nabla(\delta s) \right] d\boldsymbol{\Omega} = 0 & (17) \end{cases}$$

$$\text{where} \quad \mathbf{K}^e = \int_{\Omega_e} s^2 \begin{pmatrix} \boldsymbol{B}_0{}^T \boldsymbol{A} \boldsymbol{B}_0 + \boldsymbol{B}_0{}^T \boldsymbol{B} \boldsymbol{B}_1 + \\ + \boldsymbol{B}_1{}^T \boldsymbol{B} \boldsymbol{B}_0 + \boldsymbol{B}_1{}^T \boldsymbol{D} \boldsymbol{B}_1 + \\ + \boldsymbol{B}_s{}^T \boldsymbol{D}_s \boldsymbol{B}_s \end{pmatrix} d\Omega + \int_{\Omega_e} s^2 \begin{Bmatrix} k_w \boldsymbol{B}_3{}^T \boldsymbol{B}_3 + \\ + k_s \left(\boldsymbol{B}_4{}^T \boldsymbol{B}_4 + \boldsymbol{B}_5{}^T \boldsymbol{B}_5 \right) \end{Bmatrix} d\Omega \tag{18}$$

$$\mathbf{M^e} = \int_{V_e} s^2 \boldsymbol{L}^T \rho(z) \boldsymbol{L}\, dV \tag{19}$$

$$\begin{aligned} &\text{with} \quad \boldsymbol{B}_3 = \sum_{i=1}^{m} \begin{bmatrix} 0 & 0 & N_i & 0 & 0 \end{bmatrix}; \quad \boldsymbol{B}_4 = \sum_{i=1}^{m} \begin{bmatrix} 0 & 0 & \dfrac{\partial N_i}{\partial x} & 0 & 0 \end{bmatrix}; \\ &\boldsymbol{B}_5 = \sum_{i=1}^{m} \begin{bmatrix} 0 & 0 & \dfrac{\partial N_i}{\partial y} & 0 & 0 \end{bmatrix}; \quad \boldsymbol{L} = \sum_{i=1}^{m} \begin{bmatrix} N_i & 0 & 0 & zN_i & 0 \\ 0 & N_i & 0 & 0 & zN_i \\ 0 & 0 & N_i & 0 & 0 \end{bmatrix} \end{aligned} \tag{20}$$

The crack geometry is modeled using $\Phi(\boldsymbol{d})$, following Phuc et al. [10–13], as shown in Eq. (21).

$$\Phi(\boldsymbol{d}) = \begin{cases} 10^3 \dfrac{G_C}{4\ell_c} & \textit{if } x \le L_c \text{ and } y \le \ell_c \\ 0 & \textit{else} \end{cases} \tag{21}$$

where L_c is used to characterize the crack length.

Having solved for s via Eq. (17), the plate's natural frequency is obtained using Eq. (16).

3. RESULTS AND DISCUSSION

3.1. Validation study

To assess the accuracy and reliability of the proposed numerical formulation, an extensive validation study is conducted through comparisons with benchmark solutions reported in reputable literature. Four representative vibration problems are considered to evaluate different components of the model. These include the free vibration of porous FG

plates to verify the porous material modeling, FG plates resting on elastic foundations to confirm the foundation formulation, plates with parabolically varying thickness to examine the treatment of geometric non-uniformity, and cracked FG plates to assess the effectiveness of the phase-field approach in capturing crack-induced stiffness degradation. The excellent agreement between the present results and the reference solutions confirms the robustness and numerical soundness of the proposed model.

3.1.1. Test 1: Free vibration of porous FG plates with uniformly distributed porosity

This test considers a *Al/Al₂O₃* functionally graded square plate with uniformly distributed porosity, supported on all edges, to assess its free vibration properties. The mechanical properties adopted in this study are: for aluminium (*Al*), E_m=70*GPa*, $\upsilon_m = 0.3$, $\rho_m = 2707\ kg/m^3$; for alumina (*Al₂O₃*), E_c=380*GPa*, $\upsilon_c = 0.3$, $\rho_c = 3800\ kg/m^3$. The formula for calculating the frequency parameter in this section [19]:

$$\breve{\omega}_m = \omega h\sqrt{\rho_m / E_m} \tag{22}$$

The nondimensional natural frequency parameters obtained in the present study are compared with the reference results of Rezaei et al. [19] in Table 1. The comparison is carried out for various porosity coefficients *e* and material gradient indices *k*, showing very good agreement between the two sets of results.

Table 1. Validation of nondimensional natural frequency parameters for porous FG square plates.

e	*k* = 0			*k* = 0.5			*k* = 1		
	Present	Rezaei [19]	*Diff. (%)*	Present	Rezaei [19]	*Diff. (%)*	Present	Rezaei [19]	*Diff. (%)*
0	0.113492	0.113693	*0.18%*	0.096842	0.09651	*0.34%*	0.087304	0.087024	*0.32%*
0.2	0.115259	0.11726	*1.71%*	0.095096	0.096119	*1.06%*	0.08161	0.082444	*1.01%*
0.4	0.120127	0.122485	*1.93%*	0.093391	0.094936	*1.63%*	0.070366	0.071421	*1.48%*

3.1.2. Test 2: Free vibration of FG plates resting on an elastic foundation

In this comparative study, the free vibration response of a square FG plate resting on an elastic foundation is examined. The plate is composed of aluminum and alumina (*Al/Al₂O₃*) without porosity (*e* = 0). The material properties and the formulation adopted for evaluating the frequency parameters in this case are the same as those described in Section 3.1.1.

Table 2. Nondimensional natural frequency parameters of FG square plates on elastic foundations.

$\hat{K}_w$	$\hat{K}_s$	Method	*k* = 0	*k* = 1	*k* = 2	*k* = 5
0	0	Kumar [20]	0.0291	0.0222	0.0202	0.0191
		Present	0.029114	0.022341	0.020281	0.01921
	100	Kumar [20]	0.0406	0.0378	0.0374	0.0377
		Present	0.040611	0.037881	0.037447	0.037712
100	0	Kumar [20]	0.0298	0.0233	0.0214	0.0205
		Present	0.029803	0.023378	0.021483	0.020552
	100	Kumar [20]	0.0411	0.0384	0.0381	0.0384
		Present	0.041108	0.038502	0.038111	0.038413

Elastic foundation parameters according to Eq. (23):

$$\hat{K}_w = \frac{k_w a^4}{D_{mm}}; \qquad \hat{K}_s = \frac{k_s a^2}{D_{mm}} \quad \text{with} \quad D_{mm} = \frac{E_m h^3}{12\left(1-\upsilon_m^2\right)} \tag{23}$$

To further verify the proposed formulation, the nondimensional natural frequency parameters of square FG plates resting on elastic foundations are compared with the reference results reported by Kumar et al. [20]. The comparison is performed for different combinations of the elastic foundation parameters $\hat{K}_w$ and $\hat{K}_s$, as well as the material gradient index *k*. The results summarized in Table 2 demonstrate a close agreement between the present predictions and the available data in the literature.

3.1.3. Test 3: Free vibration of a homogeneous plate with parabolically varying thickness

In this validation example, the free vibration behaviour of a homogeneous square plate with parabolically varying thickness is investigated and compared with the reference results reported by Pilafkan and Folkow [9]. The plate is assumed to be made of *Al*, and the thickness variation follows the arched form, in which the thickness decreases nonlinearly along the plate length according to a parabolic profile.

The adopted thickness distribution is defined by $h(x) = h_0\left(1-\beta x^2/a^2\right)$, with $\beta = 1-h_a/h_0$; where h_0 and h_a denote the plate thicknesses at the left and right edges, respectively. The nondimensional frequency parameter is evaluated using the same definition as that in Ref. [9] to ensure a consistent comparison:

$$\breve{\omega}_0 = \left(\omega b^2/\pi^2\right)\sqrt{\rho_m h_0 / D_{0m}} \quad \text{with} \quad D_{0m} = \frac{E_m h_0^3}{12\left(1-\upsilon_m^2\right)} \tag{24}$$

Table 3. Nondimensional natural frequencies of aluminum plates with parabolic thickness variation.

h_0/b	β	Studies	$\breve{\omega}_{01}$	$\breve{\omega}_{02}$	$\breve{\omega}_{03}$	$\breve{\omega}_{04}$	$\breve{\omega}_{05}$
0.1	0.25	Pilafkan [9]	1.773	4.267	4.273	6.418	8.044
		Present	1.77497	4.27096	4.2641	6.57571	8.03668
	0.5	Pilafkan [9]	1.6	3.864	3.868	6.007	7.279
		Present	1.60316	3.86906	3.8676	6.00816	7.34157
0.2	0.25	Pilafkan [9]	1.647	3.668	3.671	5.354	6.359
		Present	1.64319	3.65278	3.64815	5.31813	6.16518
	0.5	Pilafkan [9]	1.504	3.138	3.224	4.745	5.96
		Present	1.50119	3.38641	3.38175	4.98432	5.93577

Table 3 presents the first several nondimensional natural frequencies for different thickness-to-length ratios and thickness variation parameters. A close agreement between the present results and those of Pilafkan and Folkow [9] is observed, demonstrating the accuracy and reliability of the proposed formulation in capturing the free vibration characteristics of plates with nonlinear thickness variation.

3.1.4. Test 4: Free vibration of cracked FG plates

In this validation example, the free vibration characteristics of cracked FG plates are examined and compared with the reference solutions reported by Huang et al. [21] and Duc et

al. [12]. The FG plate is composed of aluminium and alumina (Al/Al_2O_3), with material properties and gradation parameters identical to those adopted in the previous validation tests to ensure consistency.

The nondimensional natural frequency parameter is defined following the same formulation as in Refs. [12, 21], allowing for a direct and meaningful comparison:

$$\breve{\omega}_c = \omega\left(b^2 / h\right)\sqrt{\rho_c / E_c} \tag{25}$$

The comparison results, summarized in Table 4, show that the present predictions are in close agreement with the available data in the literature for all considered crack configurations. This agreement confirms the capability of the proposed approach to accurately capture the effects of cracking on the free vibration behaviour of FG plates.

Table 4. Nondimensional natural frequencies of cracked FG plates for different crack lengths.

c/a	Studies	Mode 1	Mode 2	Mode 3	Mode 4	Mode 5
0	Huang et al. [21]	3.925	9.787	9.787	15.62	19.49
	Duc et al. [12]	3.91454	9.79781	9.79981	15.6729	19.6359
	Present	3.92928	9.8024	9.8024	15.64	19.5489
0.1	Huang et al. [21]	3.906	9.785	9.786	15.61	19.27
	Duc et al. [12]	3.85719	9.79178	9.78391	15.615	19.0054
	Present	3.90481	9.80992	9.81961	15.6192	19.5213
0.3	Huang et al. [21]	3.725	9.581	9.76	15.56	17.53
	Duc et al. [12]	3.68898	9.55363	9.77633	15.5756	17.5406
	Present	3.72971	9.46996	9.78215	15.5122	17.8755
0.5	Huang et al. [21]	3.496	8.419	9.638	15.3	16.1
	Duc et al. [12]	3.48657	8.42352	9.68926	15.2964	16.3169
	Present	3.51617	8.05435	9.67037	15.1028	16.8198

Based on the validation studies in Sections 3.1.1–3.1.4, the developed numerical code is rigorously verified through comparisons with well-established results in the literature. The predicted natural frequency parameters exhibit excellent agreement with reference solutions for porous FG plates, plates on elastic foundations, variable-thickness plates, and cracked FG plates, with only minor discrepancies. Building on this validated framework, the code is further applied to analyze the free vibration of cracked porous FG plates with parabolically varying thickness resting on elastic foundations, as presented in Section 3.2.

3.2. Free vibration of cracked porous FG plates with parabolically varying thickness on elastic foundations

In this section, the free vibration behaviour of cracked porous FG plates with parabolically varying thickness resting on elastic foundations is investigated. The plate is composed of an Al/Al_2O_3 functionally graded material, consistent with the material system employed in the previous sections, and one plate dimension is fixed at $b = 0.6\,m$. The thickness varies along the *x*-direction according to the same parabolic profile used in Section 3.1.3: $h(x) = h_0\left(1 - \beta x^2 / a^2\right)$, with the maximum thickness $h_0 = b/50$, and the minimum thickness h_a , as illustrated in Fig. 1. A straight crack of length *c* is located at the center of the plate, while porosity is assumed to be uniformly distributed through the thickness. The plate is

assumed to rest on a two-parameter elastic foundation, whose stiffness parameters are defined in the same manner as those described in Section 3.1.2, following the formulation given in Eq. (22). The nondimensional frequency parameter is evaluated using Eq. (26), which follows the same definition as Eq. (25).

$$\breve{\omega} = \omega\left(b^2 / h_0\right)\sqrt{\rho_c / E_c} \tag{26}$$

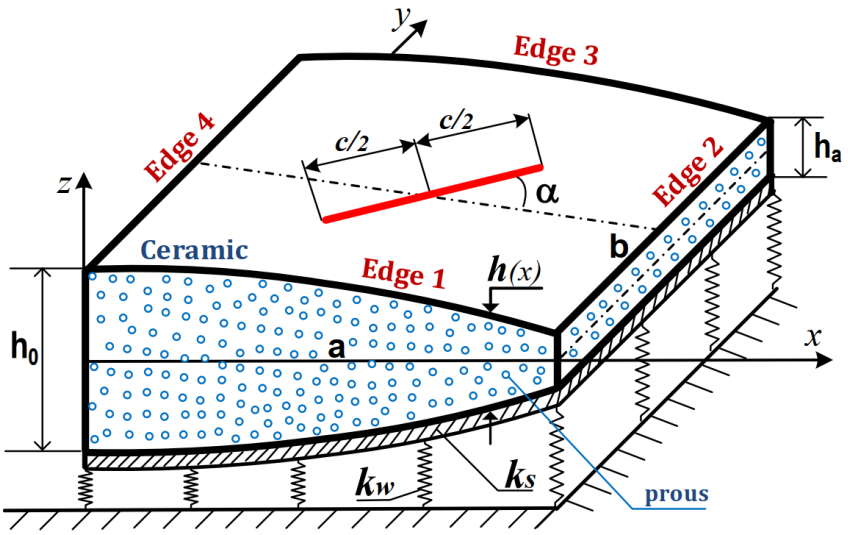

Figure 1. Geometry and crack configuration of a porous FG plate with parabolically varying thickness.

Table 5. Nondimensional frequency parameters of porous FG plates with parabolically varying thickness for different crack length ratios.

h_a / h_0	Crack length ratio (c / a)				
	0	0.1	0.3	0.5	0.7
1	4.17103	4.1492	4.02409	3.86391	3.73557
0.9	4.06192	4.04109	3.92075	3.76622	3.64229
0.8	3.95541	3.93569	3.8206	3.67235	3.55336
0.7	3.85205	3.83355	3.72424	3.58295	3.46952
0.6	3.75264	3.73549	3.63245	3.49888	3.39173
0.5	3.65837	3.64265	3.54638	3.4213	3.32124

Table 5 summarizes the nondimensional frequency parameters of a simply supported square porous FG plate with parabolically varying thickness resting on a two-parameter elastic foundation. The material system is *Al/Al₂O₃* with a material gradient index $k = 3$, and a uniform porosity coefficient $e = 0.1$. A centrally located crack with zero orientation angle $(\alpha = 0^0)$ is considered, and the foundation stiffness parameters are taken as $\hat{K}_w = 50$, and $\hat{K}_s = 5$. It is observed that, for a fixed thickness ratio h_0 / h_a, the nondimensional frequency decreases monotonically as the crack length ratio c / a increases, indicating a progressive reduction in structural stiffness due to crack growth. Likewise, for a given crack length, a decrease in the thickness ratio results in lower frequency values, owing to the combined effects of thickness thinning and material porosity. These observations

highlight the significant influence of both crack length and thickness variation on the free vibration response of porous FG plates on elastic foundations.

Table 6. Effect of aspect ratio and porosity coefficient on the nondimensional frequency parameter of FG plates.

Aspect ratio (a/b)	Porosity coefficient (e)				
	0	0.1	0.2	0.3	0.4
0.5	11.3357	11.0773	10.6997	10.0667	8.7913
0.75	5.98409	5.80614	5.54767	5.11942	4.25829
1	4.11162	3.96393	3.74909	3.39303	2.66607
1.25	3.24218	3.11006	2.91709	2.5957	1.92459
1.5	2.76487	2.6424	2.4627	2.16159	1.51789
1.75	2.47126	2.35552	2.18494	1.89741	1.26928
2	2.27488	2.16423	2.00047	1.72295	1.10505

Table 6 illustrates the influence of the aspect ratio a/b and the porosity coefficient e on the nondimensional frequency parameter of the FG plate under the conditions $h_a/h_0 = 0.75,\ k = 2,\ c/a = 0.2,$ and $\alpha = 0^0$. For a fixed aspect ratio, the nondimensional frequency decreases monotonically as the porosity coefficient increases, indicating a reduction in structural stiffness due to the presence of voids. In addition, for a given porosity level, increasing the aspect ratio a/b leads to a significant decrease in the frequency parameter, highlighting the strong effect of plate geometry on the vibration response. These results demonstrate that both material porosity and geometric configuration play important roles in governing the free vibration characteristics of FG plates resting on elastic foundations ($\hat{K}_w = 50,\ \hat{K}_s = 5$).

Table 7. Effect of crack orientation angle on the nondimensional frequency parameter of FG plates.

Crack angle (α)	Crack length ratio (c/a)				
	0	0.1	0.3	0.5	0.7
0	3.36055	3.34903	3.27518	3.17931	3.10244
15^0	3.36055	3.34908	3.27467	3.17479	3.08873
30^0	3.36055	3.36055	3.27402	3.16616	3.06027
45^0	3.36055	3.34943	3.27481	3.16399	3.04786
60^0	3.36055	3.34968	3.27772	3.1737	3.07767
75^0	3.36055	3.35017	3.2844	3.19722	3.12205
90^0	3.36055	3.35038	3.2835	3.19467	3.1204

Table 7 presents the effect of the crack orientation angle α on the frequency parameter of the square porous FG plate under the conditions $h_a/h_0 = 0.65,\ k = 4,\ e = 0.2,$ and simply supported boundary conditions (*SSSS*). The plate is assumed to rest on a two-parameter elastic foundation with $\hat{K}_w = 30$ and $\hat{K}_s = 5$. For a fixed crack length ratio c/a, the nondimensional frequency exhibits only minor variations with increasing crack angle, indicating that the influence of crack orientation is relatively weak. In contrast, for a given crack angle, the frequency parameter decreases noticeably as the crack length ratio increases, reflecting the

dominant role of crack length in stiffness degradation. These results suggest that, compared to crack orientation, crack length has a more pronounced effect on the free vibration behavior of porous FG plates on elastic foundations.

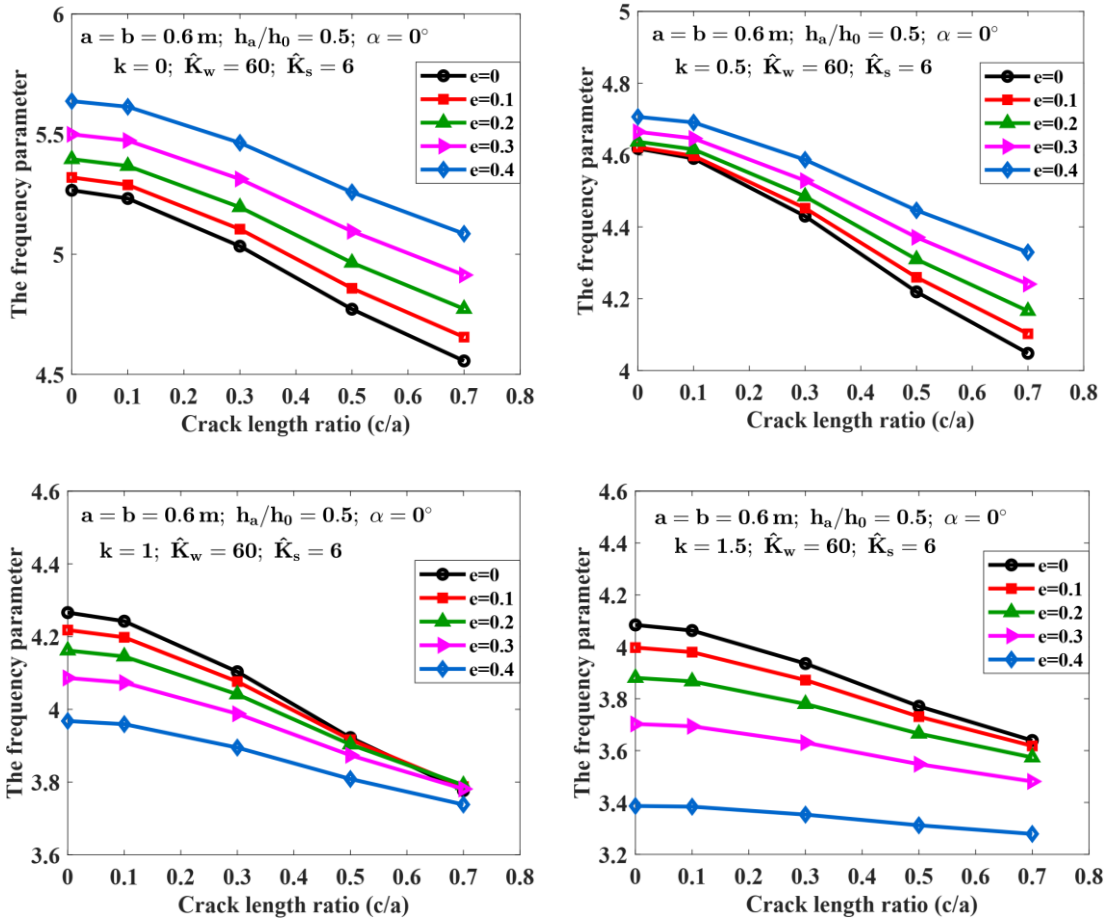

Figure 2. Influence of the porosity coefficient, material parameters, and crack length on the vibration frequency.

Figure 2 illustrates the combined effects of crack length ratio *c/a*, porosity coefficient *e*, and material gradient index *k* on the frequency parameter. For all values of *k* and *e*, the frequency decreases monotonically with increasing crack length, reflecting stiffness degradation due to crack growth. At a fixed crack length, increasing porosity generally reduces the frequency, particularly for higher *k*, indicating the softening effect of material voids. In addition, increasing the material index *k* leads to lower frequencies overall, showing that material gradation significantly influences the vibration response of cracked porous FG plates. Figure 2 also shows that for ceramic-rich plates ($k = 0$, 0.5), the fundamental frequency increases with porosity. This trend reverses for higher *k*, where metal-rich FGMs exhibit decreasing frequencies as porosity increases due to stiffness reduction.

Table 8 illustrates the frequency parameters of the square porous cracked FG plate for different crack length ratios *c/a* and boundary conditions (B.C), while the remaining parameters are kept constant. In this analysis, the square plate with the thickness ratio is $h_a / h_0 = 0.55$, the material gradient index is $k = 2.5$, and the uniform porosity coefficient is $e = 0.15$. The plate rests on a two-parameter elastic foundation with $\hat{K}_w = 40$ and $\hat{K}_s = 4$.

Table 8. Frequency parameters depending on boundary conditions at the plate edges.

B.C	Crack length ratio (c/a)				
	0	0.1	0.3	0.5	0.7
FCFF	1.21871	1.21858	1.21839	1.2183	1.2183
CFFF	1.39485	1.39469	1.39326	1.38776	1.37502
FFFC	1.63123	1.63138	1.63138	1.63137	1.63093
SSSS	3.52384	3.5084	3.4136	3.28906	3.18827
FCFC	3.5593	3.56091	3.56091	3.56091	3.55966
SCSC	4.64351	4.62952	4.53803	4.43311	4.37401
CCCC	5.71512	5.68427	5.49657	5.28764	5.16883

The boundary conditions are denoted using the edge numbering defined in Fig. 1. For example, *CSCF* indicates that edges 1 and 3 are clamped (*C*), edge 2 is simply supported (*S*), and edge 4 is free (*F*). The results show that, for all boundary conditions, the nondimensional frequency parameter decreases monotonically as the crack length ratio increases, which is attributed to the progressive loss of structural stiffness caused by crack propagation. In addition, the vibration frequency is strongly governed by the overall stiffness imposed by the boundary constraints. Plates with stiffer boundary conditions exhibit higher frequencies; hence, the fully clamped case (*CCCC*) yields the largest frequency values, while configurations with more free edges result in significantly lower frequencies. Notably, among the cases *FCFF*, *CFFF*, and *FFFC*, which each include only one clamped edge, the *FCFF* configuration leads to the lowest frequencies. This behaviour can be explained by the fact that the clamped edge in *FCFF* is located at the region of minimum thickness, thereby providing less effective stiffness and making the plate more prone to instability compared with the other configurations.

Table 9 reports the nondimensional frequency parameters of a cracked square porous FG plate for different crack length ratios c/a and elastic foundation stiffnesses. The plate is simply supported on all edges (*SSSS*), with thickness ratio $h_a/h_0 = 0.75$, gradient index $k = 1.5$, porosity coefficient $e = 0.22$, and crack orientation $\alpha=0^0$.

Table 9. Frequency parameters depending on the elastic foundation.

$\hat{K}_w$	$\hat{K}_s$	Crack length ratio (c/a)				
		0	0.1	0.3	0.5	0.7
0	0	3.39655	3.37483	3.24761	3.0754	2.93071
100	0	3.78911	3.76963	3.65601	3.5038	3.37748
	10	4.46575	4.45303	4.36975	4.26223	4.17616
	50	6.49346	6.49529	6.46708	6.42751	6.39287
	100	8.35667	8.36825	8.369	8.35747	8.33913
500	0	5.06264	5.04802	4.96329	4.85185	4.76134
	10	5.58568	5.57549	5.50892	5.4237	5.35618
	50	7.30652	7.30816	7.28302	7.24774	7.21688
	100	9.00184	9.01261	9.01328	9.00247	8.98534

For a fixed foundation stiffness, the frequency parameter decreases as the crack length increases due to stiffness degradation. In contrast, increasing $\hat{K}_w$ and $\hat{K}_s$ significantly raises

the frequencies, demonstrating the strong stiffening and stabilizing effect of the elastic foundation. Moreover, this enhancement reduces the sensitivity of the vibration response to crack growth, especially at higher foundation stiffness levels. As a result, the adverse influence of cracking is partially mitigated by the elastic support, leading to a more stable dynamic behaviour of the plate.

4. CONCLUSION

This study presents a comprehensive free vibration analysis of cracked porous functionally graded material (FG) plates with parabolically varying thickness resting on two-parameter elastic foundations. The formulation integrates the first-order shear deformation theory with a phase-field approach for crack representation and a finite element implementation, allowing cracks to be modelled without remeshing while maintaining numerical robustness.

The novelty of the present work lies in the unified treatment of several key features that have rarely been considered simultaneously in existing studies, including material gradation, uniformly distributed porosity, parabolically varying thickness, arbitrary crack length and orientation, and Winkler–Pasternak elastic foundations. Based on the validated framework, extensive parametric investigations were performed. The results reveal that increases in crack length, porosity coefficient, thickness reduction, and material gradient index generally reduce the natural frequencies due to stiffness degradation. In contrast, stiffer boundary conditions and higher foundation stiffness parameters significantly enhance the vibration frequencies and effectively mitigate the detrimental effects of cracking. The influences of crack orientation and plate aspect ratio are also quantified and shown to be secondary compared to crack length and foundation stiffness. Overall, the proposed model provides an effective and versatile tool for predicting the dynamic behaviour of advanced cracked porous FG plates under complex mechanical and support conditions.

ACKNOWLEDGMENT

This research is funded by University of Transport and Communications (UTC) under grant number T2025-CB-014TĐ.

REFERENCES

[1]. H. H. Le, N. V. Nguyen, D. H. Phan, T. D. Nguyen, Nonlinear free oscillation of tri-directional functionally graded porous skew plates with variable thickness in high-thermal environment, Case Studies in Thermal Engineering, 70 (2025) 106101. https://doi.org/10.1016/j.csite.2025.106101
[2]. N. V. Nguyen, D. H. Phan, Nonlinear free vibration of bi-directional functionally graded porous plates, Thin-Walled Structures, 192 (2023) 111198. https://doi.org/10.1016/j.tws.2023.111198
[3]. T. Assas, M. Zitouni, H. Bourada, Static, free vibration, and buckling analysis of functionally graded plates using the strain-based finite element formulation, Archive of Applied Mechanics, 94 (2024) 2243–2267. https://doi.org/10.1007/s00419-024-02635-0
[4]. E. Yıldırım, Effect of the porous structure on the hygrothermal vibration analysis of functional graded nanoplates, Acta Mechanica, 235 (2024) 5079–5106. https://doi.org/10.1007/s00707-024-03990-3
[5]. P.Kumar, R.Sharma, S.Singh, Thermoelectrical vibration and bending analysis of multidirectional functionally graded circular piezoelectric porous sigmoid plate, International Journal of Mechanical and Materials Design, (2025). https://doi.org/10.1007/s10999-025-09779-z

[6]. S. Jandaghi-Semnani, R. Attarnejad, R. Kazemi-Firouzjaei, Free vibration analysis of variable thickness thin plates by two-dimensional differential transform method, Acta Mechanica, (2013). https://doi.org/10.1007/s00707-013-0833-2
[7]. G. P. Sinha, B. Kumar, Frequency analysis of variable thickness Kirchhoff plates by isogeometric approach, Journal of The Institution of Engineers (India), Series C, 104 (2023) 271–280. https://doi.org/10.1007/s40032-023-00910-7
[8]. S. R. Farsani, Z. Saadat, R.-A. Jafari-Talookolaei, R. Tikani, S. Ziaei-Rad, Free vibrational analysis of variable thickness plate made of functionally graded porous materials using internal supports in contact with bounded fluid, Ocean Engineering, 263 (2022) 112335. https://doi.org/10.1016/j.oceaneng.2022.112335
[9]. R. Pilafkan, P. D. Folkow, Free vibration analysis of rectangular plates with variable thickness using a meshless method, Forces in Mechanics, 21 (2025) 100328. https://doi.org/10.1016/j.finmec.2025.100328
[10].P. M. Phuc, Analysis free vibration of the functionally grade material cracked plates with varying thickness using the phase-field theory, Transport and Communications Science Journal, 70 (2019) 122–131. https://doi.org/10.25073/tcsj.70.2.35
[11].P. M. Phuc, Using phase field and third-order shear deformation theory to study the effect of cracks on free vibration of rectangular plates with varying thickness, Transport and Communications Science Journal, 71 (2020) 853–867. https://doi.org/10.47869/tcsj.71.7.10
[12]. P. M. Phuc, D. T. Manh, N. D. Duc, Free vibration of cracked FG plates with variable thickness resting on elastic foundations, Thin-Walled Structures, 161 (2021) 107425. https://doi.org/10.1016/j.tws.2020.107425
[13]. P. M. Phuc, N. D. Duc, Free vibration of cracked MEE FG plates resting on elastic foundations using phase-field simulation, Journal of Engineering Mechanics, 149 (11) (2023) 04023103. https://doi.org/10.1061/JENMDT.EMENG-7088
[14].B. K. Chandrakar, N. K. Jain, Ankur Gupta, Nonlinear vibration analysis of a cracked isotropic plate with varying thickness coupled with fluid, Journal of the Brazilian Society of Mechanical Sciences and Engineering, 2025. https://doi.org/10.1007/s40430-025-05616-8
[15].L. Kurpa, R. Lewandowski, A. Żur, Free vibration analysis of porous functionally graded material plates with variable thickness on an elastic foundation, Mathematics and Computers in Simulation / Mathematics and Computational Applications, 29 (2024) 10. https://doi.org/10.3390/mca29010010
[16].M. C. Srivastav, A. K. Barik, S. Chakraverty, Analysis of free vibration characteristics of porous FG skew plate using meshfree approach, Multiscale and Multidisciplinary Modeling, Experiments and Design, 7 (2024) 6245–6261. https://doi.org/10.1007/s41939-024-00576-3
[17].M. Izadi, M. Abedi, P. S. Valvo, Free vibration analysis of a functionally graded porous triangular plate with arbitrary shape by isogeometric approach, Thin-Walled Structures, 205 (2024) 112422. https://doi.org/10.1016/j.tws.2024.112422
[18].Y. Xue, C. Zhang, K. Shi, Y. Gao, Z. Gao, Free vibration analysis of functionally graded porous corrugated plates with porosity distributions in the thickness and width directions, Advances in Engineering Software, 212 (2026) 104066. https://doi.org/10.1016/j.advengsoft.2025.104066
[19].A. S. Rezaei, A. R. Saidi, M. Abrishamdari, M. H. Pour Mohammadi, Natural frequencies of functionally graded plates with porosities via a simple four-variable plate theory: An analytical approach, Thin-Walled Structures, 120 (2017) 366–377. https://doi.org/10.1016/j.tws.2017.08.003
[20].V. Kumar, S. J. Singh, V. H. Saran, S. P. Harsha, Vibration characteristics of porous FG plates with variable thickness resting on Pasternak's foundation, European Journal of Mechanics – A/Solids, 85 (2021) 104124. https://doi.org/10.1016/j.euromechsol.2020.104124
[21].C. S. Huang, P. J. Yang, M. J. Chang, Three-dimensional vibration analyses of functionally graded material rectangular plates with through internal cracks, Composite Structures, 94 (2012) 2764–2776. https://doi.org/10.1016/j.compstruct.2012.03.012